Multi-purpose interfaces for coupling SPH with other solvers

Bouscasse B.
CNR-INSEAN
Rome, Italy

Marrone S.
CNR-INSEAN
Rome, Italy

Colagrossi A.
CNR-INSEAN
Rome, Italy

Di Mascio A.
CNR-IAC
Rome, Italy

***Abstract*—An algorithm for coupling SPH with an external solution is presented. The external solution can be either another SPH solution (possibly with different discretization) or a different numerical solver or an analytical solution.**

The interaction between the SPH solver and the external solution is achieved through an interface region. The interface region is defined as a fixed portion of the computational domain that provides a boundary condition for the SPH solver. A ghost fluid, composed by fully lagrangian particles (*i.e.* ghost particles) covering the interface region, is used to impose the boundary condition. The ghost particle evolution, including its position, is integrated in time according to the field of the external solution. The physical quantities of the ghost particles needed in the integration scheme are obtained through an MLS interpolation on the field of the external solution. When a ghost particle crosses the boundary of the interface region, entering in the SPH domain, it evolves according to the SPH governing equation.

The spatial distribution of the ghost particles can become largely non-uniform due to the forcing by the external solution. Thus, a packing algorithm is applied on the ghost particles in the interface region, to guarantee a particle distribution suitable for SPH operators. Since the ghost particles can exit from the interface region, a seeding algorithm is needed to introduce new ghost-particles.

The algorithm is tested on several benchmarks and with the external solutions given by other SPH solvers with different discretizations and by analytical solutions. The technique is deeply investigated in terms of accuracy, efficiency and possible applications. Finally a coupled simulation involving a finite volume solver is presented.

I. Introduction

Meshless methods and, among them, Smoothed Particle Hydrodynamics (SPH) are nowadays well validated options in order to tackle hydrodynamic problems. Some of their features are equivalent to mesh based solvers, and the free surface treatment results easier. One of the most important gaps to bridge is the possibility to use different resolutions in the same calculations. In mesh based methods, techniques as mesh stretching or even multi-block techniques are widely used. This concedes a consequent advantage to calculate boundary layers or more generally in large computational domain. Within the SPH framework, the equivalent to stretching, implemented through a variable-h kernel formulation was introduced by [1] (see also [2]). The kernel size evolves along the domain together with the particle size. The technique is interesting for short simulations where there is no strong mixing, but can lead to stability problems for numerical evolutions over a larger time. A recent achievement is the splitting coalescing scheme presented in [3] following the initial idea of [4] and later study of [5]. Another interesting topic is the coupling of numerical methods, often known as domain decomposition. SPH has been coupled with mechanical model [6], FEM for fluid structure interaction [7], some attempts have also been made to couple with shallow water solution [8].

In the present paper a complete procedure is presented to permit the interfacing of SPH with another numerical solution. It aims to show the capability to divide the numerical domain in subdomains solved by different numerical solvers. This external - from the point of view of the single SPH domain - solution can be either an other SPH calculation or a result obtained with a different technique. This approach theoretically allows full coupling with the external solution and several tests are performed in this goal. Among those the results of the coupling with a finite volume solver are presented.

II. Modeling multi-domain interaction in SPH

The aim of the present work is to provide a full coupling of the SPH solver with an external numerical solver. This means that the solution coming from the external solver has to be used as boundary condition of the SPH solver, and viceversa. The transfer of the external solution to the SPH solver is achieved through an interface region. The interface is defined as a region (area) of the computational domain that provides a boundary condition for the SPH solver imposed by an external solution. The boundary conditions are imposed through the ghost fluid, that is composed by fully lagrangian particles. They cover the whole interface region and evolve according to the field given by the external solution. Then the SPH solution is transferred to the external solver through interpolation of the particle data in a specular manner. The imposition of a generic boundary condition given by an external solver requires the definition and development of specific algorithms that allow for a general representation of the fluid field in the interface region. In the following sections some dedicated procedures are described.

A. Definition of the domain components

Consider a generic fluid domain D, delimited by a closed boundary ∂B (see figure 1). The generic boundary ∂B can be split into several parts, depending on the condition applied

on each section. Some boundaries correspond to physical boundaries as in the case of solid surfaces, and some others are artificial boundaries added for numerical purposes (for example, the fluid domain can be divided into several subdomains, the solution being given by different solvers in each subdomain).

Each boundary section is either penetrable or non-penetrable (fluid can cross or not the boundary). Non-penetrable boundaries are typically a no-slip $U_{\partial B} = 0$ or a free-slip wall $\vec{U}_{\partial B} \cdot \vec{n} = 0$ whereas a penetrable boundary means that there exists an incoming and/or outcoming flow with imposed characteristics. For example, if the domain is divided in two subdomains solved by different numerical solvers or using different numerical parameters, the boundary between the two subdomains is generally penetrable ($\vec{U}^{D1}_{\partial B} = f(x,t)$ and $p^{D1}_{\partial B} = g(x,t)$).

Different difficulties arise when enforcing a boundary condition in an Eulerian framework or in a Lagrangian one. For example, boundary condition for a free-surface can be treated in a more easy way in a Lagrangian context. Conversely No-slip and free-slip wall condition are not easy to impose in the SPH context. The ghost fluid technique is a possible solution (i.e. an extension of the fluid over the boundary) (see e.g. [9], [10], [11]). The ghost fluid technique can be used also for penetrable boundary condition, for example when enforcing periodic condition of inflow and outflow of flow currents (see e.g. [12]).

The coupling with an external solution using ghost fluid is the object of the investigation that follows. This is performed through an interface that is conceptually a region dedicated to receiving communication from an outer solution.

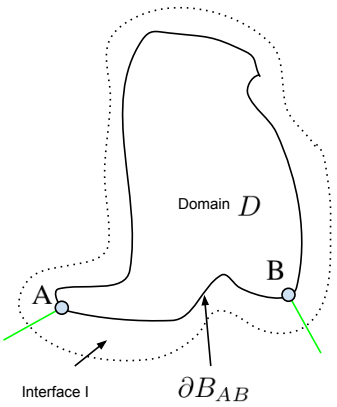

Fig. 1. A generic fluid domain with a generic interface

A sketch of a generic multi-domain decomposition is shown in figure 2. Some boundaries are solid surfaces, some other are artificial boundaries that split the whole fluid domain, D, in different subdomain $D1 \cup D2 \cup D3$. As depicted in figure 2, overlapping between subdomains can be considered; for example, a part of the boundary of D1 is inside D2 and viceversa. As shown later, overlapping may be useful for an easier design of the computational domain or for numerical reasons.

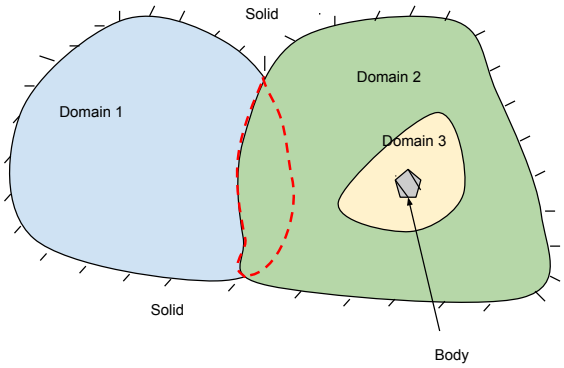

Fig. 2. A domain divided in three different subdomains.

B. Description of the numerical interface

As stated above, the interface is composed by a continuous boundary and the associated ghost fluid region. A sketch of a generic interface is presented in figure 3 for generic boundary from point A to point B (∂B_{AB}). The width of the ghost region has to be larger than the radius of the interpolation kernel (2h or 3h depending by the kernel function choice). A point in the ghost region, closer to the boundary ∂B_{AB} than any other boundary, belongs to the interface connected to the boundary ∂B_{AB}.

The ghost fluid regions need to be discretized with particles, whose position can be fixed in space when considering solid surfaces (as shown in [13]). In this case, the flow quantities in the ghost fluid region are set depending on the boundary condition involved using specific rules, as shown in [13] and in [11].

Conversely, when the boundary ∂B_{AB} is crossed by a flow, the ghost particles can move with a prescribed time law. For example, in the simulation of open channel flow with inlet and outlet interfaces (see [12]), the boundary is penetrable and the ghost-fluid particles move with the imposed values. This allows mass transfer across the boundary and the ghost particles are transformed in fluid particles when crossing ∂B_{AB}, as well as real fluid particles need to become ghost particles when entering through the interface.

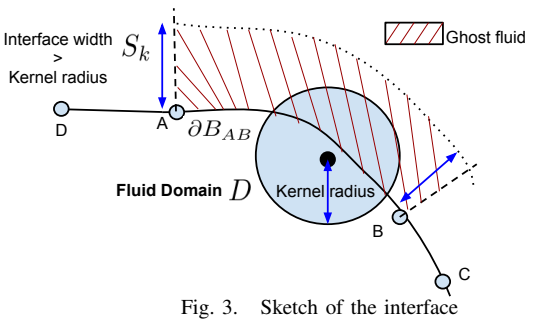

Fig. 3. Sketch of the interface

C. Initialization of the computation

For each particle, a signed distance ϕ_k is evaluated from each section of the k-th boundary (including the free surface). All the boundaries are oriented in such a way that the fluid region belongs to the right side; this allows to define a sign to the ϕ_k function. When all the distance ϕ_k are positive, the particle is assigned to the fluid. If one or more ϕ_k is negative, the particle is associated to the interface connected to the closest boundary. For those associated with an interface, if their distance to the boundary is less than the width originally set for the interface, S_k, they belong to the ghost fluid region; conversely, they are kept as frozen particles. The particles whose distance is larger than the sum of width S_k plus the kernel radius are eliminated. This initial procedure allows also to count the ghost particles that fill each interface region. The frozen particles are kept attached to the interface during all the calculation, but they are used only during the regularization procedure (see section III-A). The sketch of a typical interface is shown in figure 4.

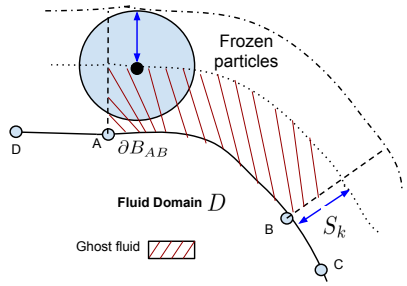

Fig. 4. Sketch of the interface with frozen particles used during the regularization procedure (see section III-A)

III. Description of the coupling algorithm

As described previously, the interfaces are characterized by artificial boundary ∂B_{AB} crossed by fluid when different domains are coupled. In such a condition, the conservation of mass and momentum (which is intrinsically satisfied in the SPH scheme) need to be handled in a suitable manner, as the fluxes of mass and momentum across the artificial boundary are calculated accurately only if the sum of the particle volumes matches exactly the volume of the interface region. Furthermore, the ghost particles have to be distribuited in a regular way to avoid depletions in the SPH interpolation and inaccuracies of the differential operators. These two requirements (correct mass/volume in the interface and an homogeneous distribution of the particles) are not naturally fulfilled in presence of mass fluxes. If more ghost particles are transformed in fluid particles than viceversa, it leads necessarily to a lack of particles in the interface (see figure 5).

In some specific cases, when fluxes across the artificial boundary k have a periodic behaviour in time, it can be sufficient to set the width of the k-th interface, S_k, large enough to ensure that at least a strip of width equal to the kernel radius is always filled. In this way the particles would go in and out the fluid domain without the need of performing any operation on the ghost particles.

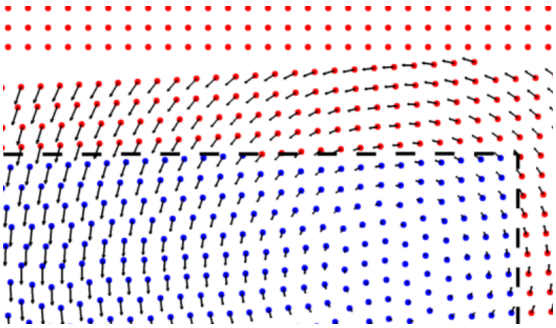

Fig. 5. Example where particles are missing in the interface because of the lagrangian evolution.

A. Control of the particle distribution in the interface through seeding, removing and packing procedures

At each time step the distribution of particles is checked at the different interfaces, and only when the spatial distribution is correct, the scheme can advance to the interpolation and integration procedure. The verification is achieved simply by counting the ghost particles populating the interface and comparing it to the number obtained originally during the initialization procedure. If the variation of the particle number is below a threshold of $2-5\%$, the interface is considered correctly filled. More accurate criteria could be used (*e.g.* local check of lack of mass through kernel summation) but it is leaved for further investigation. In the general case, lack of mass at the interfaces and spatial disorder develop in time (as shown in figure 5) and three operations are needed to recover particle distribution. The first operation is the seeding of particles in the interface in case of lack of particles, the second is the removing of particles when they leave the area of interest behind the interface and the third is the regularization of the updated set of ghost particles. For the seeding procedure, if particles are missing, the number that has to be inserted in the interface is evaluated. To this purpose, when the interface is created, the whole interface region is filled with seed points with spacing equal to the ghost particle size and distributed on a cartesian lattice. Through the kernel based interpolation, the density is calculated on the seed points and then they are sorted by their density value. If n-particles are missing at the interface, the first n-seed points are inserted as new ghost particles. In figure 6, the interface is depicted after the seeding. The particle removal is straightforward: at each time step if any ghost particle in the interface move away to a distance from the boundary larger than S_k, it is eliminated. After the seeding/removal procedure the number of filling particles is correct but their spatial distribution is not.

The spatial distribution of the particles has to be as homogeneous as possible. To this aim a packing procedure developed in [14] is applied inside the interface when the particles have

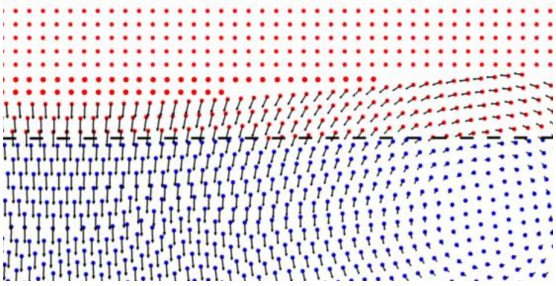

Fig. 6. Seeding of missing particles on carthesian grid. Packing will follow for regularization.

to be regularized. This procedure requires the use of frozen particles in order to enforce the boundary conditions. That is the reason of keeping frozen particles (subsection II-C) in each interface and, for the same reason, also the real fluid as well as the ghost fluid particles of the neighbouring interfaces are frozen during the packing procedure. An example of the distribution of the particles after the packing procedure is presented in figure 7. The packing procedure can implies a non negligible increase of the computational cost. However, the relative time with respect to the whole simulation reduces with the resolution since this procedure involve only the boundaries of the fluid domain. However, time optimisation of the packing operation should be object of future investigation.

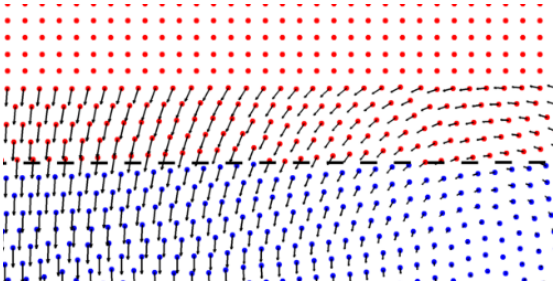

Fig. 7. Particles distribution after the seeding and packing. Interpolation and time intergration will follow.

B. Data Interpolation for communication with an external solution

With the procedure precedently described, the interfaces are always filled with ghost particles regularly spaced. The physical values of the ghost particles has to be set as function of the solutions defined in the other subdomains.

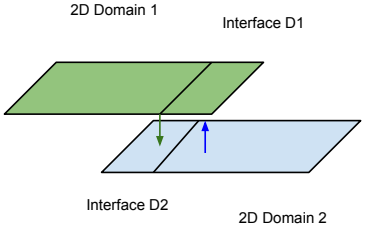

Fig. 8. Two domains communicating through their two interfaces

For example, in sketch 8 a fluid domain divided in two subdomains D_1 and D_2 is depicted. The two subdomains are connected to each other by two interfaces, whoses boundaries in general can be different (overlapped subdomains). In D_1 the problem is solved by an SPH scheme, while in the second subdomain, D_2, the solution is given by a generic second solver not specified here. The values on the SPH particles at the interface of the D_1 are interpolated from the values inside D_2 with a technique depending on the topological characteristics of the solution. For example, if in D_2 the solution if given by an analytic solution, the set $[p, \vec{u}]$ on the ghost particles will be given by its evaluation at the particle positions. If solution in D_2 is given on a mesh, $[p, \vec{u}]$ will be evaluated through an interpolation technique depending by the mesh topology used (e.g. cartesian grid, unstructured grids, etc.). The solution in D_2 can be also given by another SPH scheme with different numerical characteristics with respect the one adopted in D_1. In such a case, the set $[p, \vec{u}]$ on the ghost particles will be interpolated using the SPH kernel adopted in D_2 through an MLS (moving least square) [15] interpolation on the D_2 field.

C. Time integration

The time integration for the SPH sheme is performed with a Runge Kutta 4-th order scheme and the values of the ghost particles in the interfaces are then updated each substep (similarly to what is shown in [12] for an inflow outflow problem and in [16] for fluid/body interaction). In the interfaces the ghost particle evolution, including its position, is integrated in time according to the field of the external solution.

IV. Taylor-Green vortex

The Taylor Green vortex is an unsteady flow of a decaying vortex, which has an exact closed form solution of the incompressible Navier Stokes equations. The fluid domain is a square $[0, 2\pi L] \times [0, 2\pi L]$, defined the Reynold number as Re$= U\, 2\pi L\, \nu$. Periodic boundary condition are enforced on domain boundary and the solution is given, for the non-dimensional variables, by:

$$\begin{aligned} u &= \sin x \cos y\, e^{(-8\,\pi^2/Re)\,t} \\ v &= \cos x \sin y\, e^{(-8\,\pi^2/Re)\,t} \\ p &= \tfrac{1}{2}\left[\, \cos(2\,x) + \cos(2\,y)\,\right] e^{-16\pi^2/Re\,t} \end{aligned} \tag{1}$$

where the reference length and time are respectively L, $2\pi L/U$, being U the maximum velocity in the initial conditions while the pressure is made non-dimensional through $\rho U^2/2$.

Simulations are done within two setups presented in figure 9. In the first, the SPH is used in the whole fluid domain $[0, 2\pi\, L] \times [0, 2\pi\, L]$ enforcing the periodic boundary conditions. In the second simulation the fluid domain is divided in two subdomains D_1 and D_2. In the first subdomain the SPH is used while the solution in D_2 is known analytically through equation (1). The value of $[p, u, v]$ for the ghost particles of the

interfaces of D_1 are therefore given also analytically. With this second numerical setup the artificial boundaries can be drawn arbitrarily. For example the simulation is here done with five boundaries associated with five interfaces.

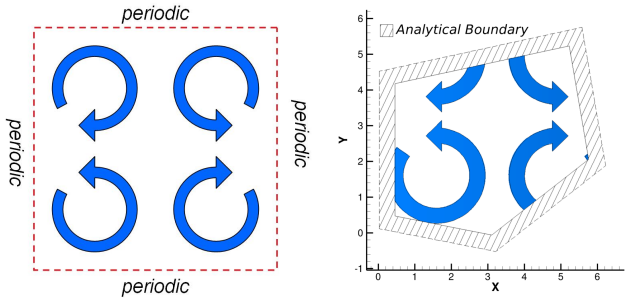

(a) Case I (b) Case II

Fig. 9. Sketches of the two simulations of the Taylor-Green flow (right: square domain with periodic boundaries, left: domain with analytical boundaries)

The results from the two simulations are compared in terms of vorticity and velocity. An instant color map of the vorticity, obtained in the simulation with squared domain, is depicted in figure 10, whereas the same data for the asymetric domain is presented in figure 11. The differences are very limited. A second comparison is done with the horizontal velocity interpolated on a horizontal cut, and the vertical velocity interpolated on a vertical cut. The results shown in figure 12 confirm that the two calculations are almost identical.

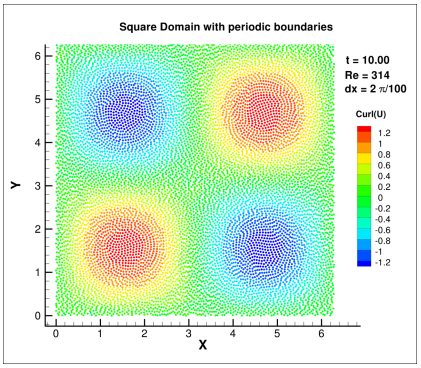

Fig. 10. Simulation results of the Taylor-Green flow (square domain with periodic boundaries)

V. Poiseuille flow

The Poiseuille flow was chosen as a test case for the validation of the splitting/coalescing scheme in [3]. The tests are reproduced in order to validate the present procedure. The Reynolds number set for this calculation is Re $= \frac{U_0 d}{\nu} = 20$ and initial particle distribution is given by the packing procedure.

A. Single domain with periodic condition or interface with analytical solution

The first tested issue is the capability to reproduce with the analytic interface the results obtained with a periodic

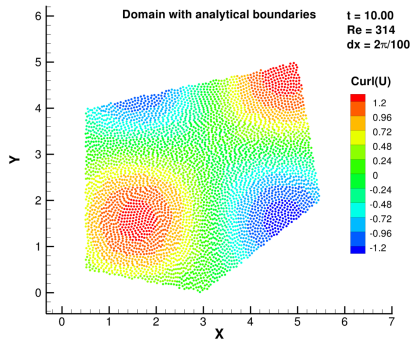

Fig. 11. Simulation results of the Taylor-Green flow (domain with analytical boundaries)

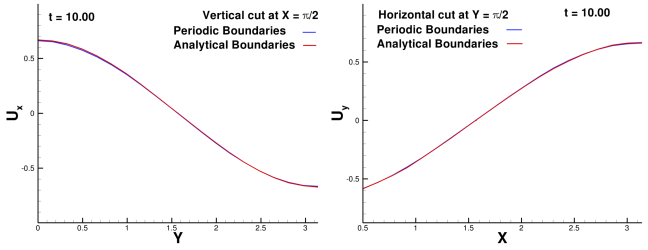

Fig. 12. Taylor green. Periodic and Analytic boundary condition, comparison of the horizontal and vertical velocities.

simulation. With the analytic procedure, the seeding and packing process is performed frequently and, a priori, this could cause some errors in the solution. This test case is set up in order to evaluate the numerical noise possibly introduced in the field by the successive operations of seeding and packing. The time history of the transversal velocity is plotted in figure 13. The results for both longitudinal and transversal velocities are summarized in table V-A.

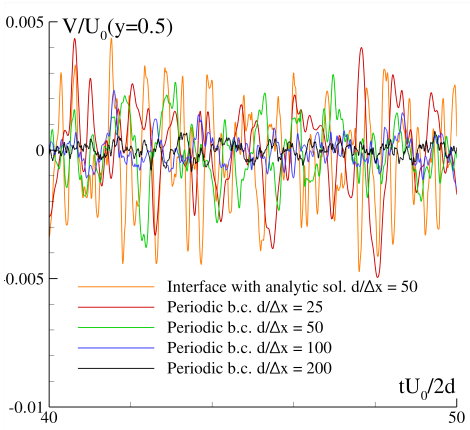

Fig. 13. Poiseuille flow. Periodic b.c and interface with analytical solution. Time evolution of the spurious transversal velocity at $y = 0.5$

Value at y=0.5	Mean $\frac{U}{U_0}$	Std $\frac{V}{U_0}$	Mean $\frac{U}{U_0}$	Std $\frac{V}{U_0}$
$tU_0/2d$	[5:20]	[5:20]	[40:50]	[40:50]
Periodic b.c $d/\Delta x : 50$	1.02	0.0009	1.013	0.0012
Interface $d/\Delta x : 50$	0.99	0.0019	0.992	0.0019

TABLE I
PERIODIC AND ANALYTIC IN/OUTFLOW. MEAN VALUE OF LONGITUDINAL VELOCITY AND STANDARD DEVIATION OF THE TRANSVERSAL VELOCITY.

B. Periodic boundary condition with a second SPH internal domain

In this case, a second SPH domain is inserted in the middle of the fluid domain. The domain are designed as shown in the sketches 14 and 15. The resolution of the internal domain is changed as described in column 2 and 3 of table V-B.

The longitudinal velocity is plotted in figure 16. The values are taken from the internal domain at $x = 0.5d$ and $y = 0.5d$. The time evolution in different from the one obtained in the previous case. In particular the results are poor in the case of the lower resolution $d/\Delta x = 25$, but the agreement with the theoretical value $U = U_0$ increases as Δx decreases.

The results are summarized in table V-B. As in the first setup, the standard deviation of the transversal velocity is taken as a measurement of the numerical noise. It is observed that the latter diminishes with the increasing resolution and remains always limited.

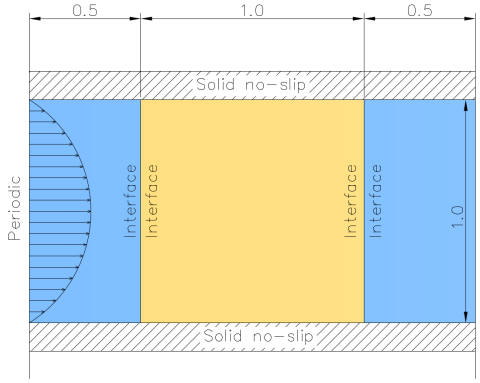

Fig. 14. Sketch of the double domain simulation of the Poiseuille flow.

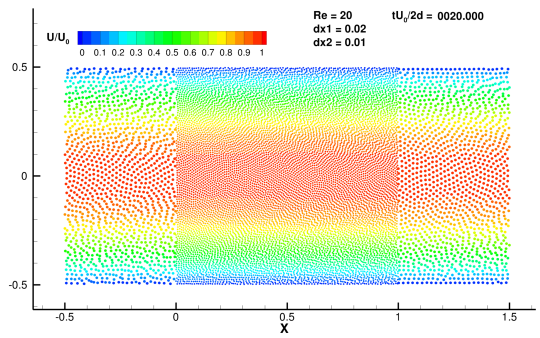

Fig. 15. Simulation of the Poiseuille flow with double SPH domain. Particles are colored accroding to their longitudinal velocity.

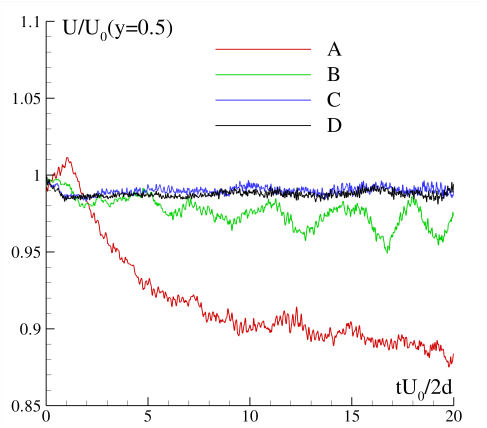

Fig. 16. Double domain Poiseuille flow. Time evolution of the velocity at $y = 0.5$

y=0.5	$d/\Delta x$ ext	$d/\Delta x$ int	Mean U	Std V
A	25	25	0.90	0.0021
B	50	50	0.97	0.0015
C	50	100	0.99	0.0012
D	50	200	0.99	0.0010

TABLE II
MEAN VALUE OF LONGITUDINAL VELOCITY AND STANDARD DEVIATION VALUE OF THE TRANSVERSAL VELOCITY, $5 < tU_0/2d < 20$

VI. STANDING WAVE

A. Double SPH Domain

An extensive analysis about the SPH calculation of a standing wave is treated in [17]. This test case is particularly appropriate to measure the numerical dissipation of a numerical procedure. The Reynolds number is fixed at Re=1500. The simulation is performed with two SPH domains at different resolutions. The reference solution is given by [18]. Firstly, the simulation is performed without removal nor seeding of ghost particles. As a consequence, the packing procedure is not performed. As mentioned in section III, this is possible because the flow crossing the interface is periodic. A conservative choice for the interface width is the amplitude $a = 0.1\lambda$ of the standing wave that, for the considered cases, is set equal to 0.1. Figure 18 shows the kinetic energy decay for the case without seeding and packing. A second test case is performed with removal and seeding of ghost particles (and, consequently, packing procedure). The same results are shown in figure 19. In both configurations, the convergence towards the analytical solution in very good; this proves the very low dissipation introduced by the interpolation procedure (first case) and the seed and packing procedure (second case).

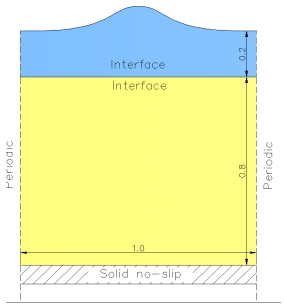

Fig. 17. Standing wave. Sketch of the numerical domain

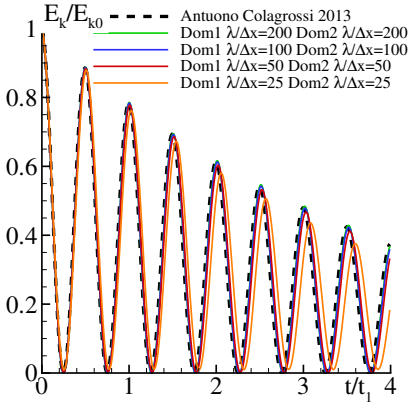

Fig. 18. Standing wave. Time evolution of the kinetic energy for the case without packing and seeding

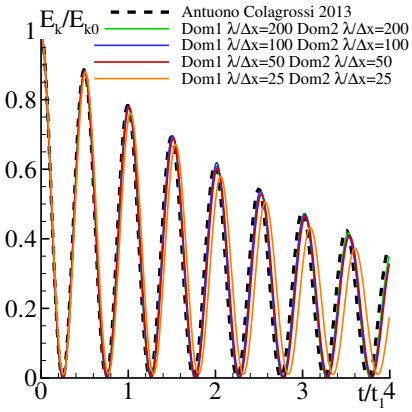

Fig. 19. Standing wave. Time evolution of the kinetic energy for the case with packing and seeding

B. Coupling with a Finite Volume Solver

The standing wave test case is finally used in order to test the coupling between SPH and a finite volume solver ([19], [20]). This case represents a quite demanding test since the considered solvers are radically different, the finite volume solver (FVS in the following) relies on an incompressible implicit scheme written in Eulerian formalism while the SPH solver is lagrangian, weakly-compressible and explicit in time. The numerical domain is depicted in figure 20. The geometry

$\lambda/\Delta x$ Dom1	$\lambda/\Delta x$ Dom2	Error
25	25	1.1
50	50	0.5
100	100	0.3
200	200	0.3
100	200	0.2

TABLE III
ERROR OBTAINED FOR THE RESULTS WITHOUT SEED AND PACKING IN THE INTERFACE, $0 < t < 10$

$\lambda/\Delta x$ Dom1	$\lambda/\Delta x$ Dom2	Error
25	25	1.2
50	50	0.5
100	100	0.4
200	200	0.3
100	200	0.3

TABLE IV
ERROR OBTAINED FOR THE RESULTS WITH SEED AND PACKING IN THE INTERFACE, $0 < t < 10$

of the mesh used for the FVS is on the left. The coloured part (bottom) corresponds to the flow calculated by the FVS whereas the grey is interpolated from the SPH solver. The same convention is used for the SPH domain. The *CHIMERA* multi-block features of the the FVS makes easy to have a low resoluted mesh over the whole fluid domain. Differently to what was shown in the double domain SPH-SPH of the precedent section, the FVS mesh and the SPH particles are slightly overlapped in order to increase the numerical stability.

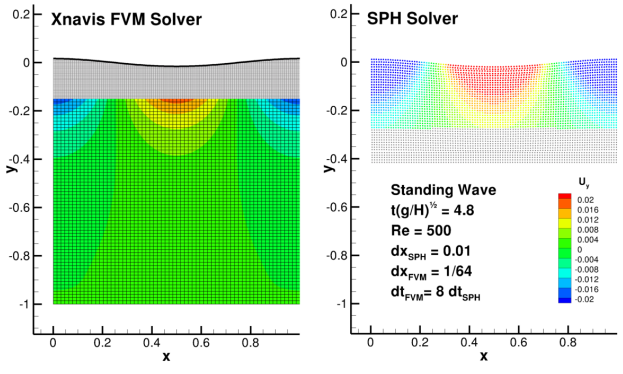

Fig. 20. Standing wave. Right: FV mesh, left: SPH particles, the colored part is calculated, grey is obtained from other domain.

Some convergence tests are performed on the Kinetic Energy decay and on the Enstrophy time evolution for the case Re=500. The results depicted in figure 21 and figure 22 show a convergence of the two quantities.

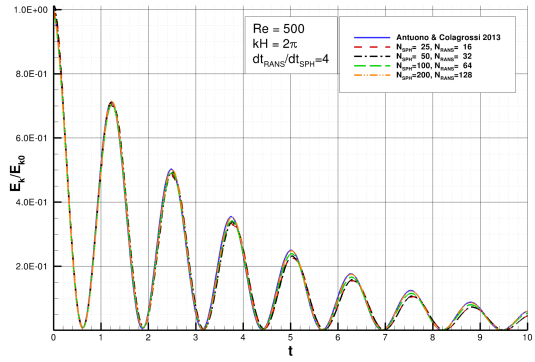

Fig. 21. Standing wave. Time evolution of the enstrophy for the case with coupling with FVM solver

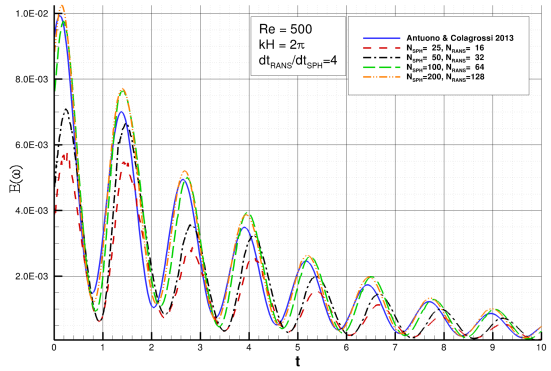

Fig. 22. Standing wave. Time evolution of the enstrophy for the case with coupling with FVM solver

VII. Conclusion

A complete procedure aiming to couple SPH domain with external solution is shown. The complexities related to the lagrangian features are overcome by using numerical interfaces. Great care is necessary to maintain the distribution of ghost particles in the interface always uniform. The packing algorithm precedently described shows to be effective to this aim. The numerical error given by the procedure is carefully evaluated for simple well-controlled test cases. Globally the results obtained with multi domain converge on the single domain solution. The technique is satisfactorily applied for SPH multi-resolution, and finally a more complex coupling is done with a finite volume solver.

Acknowledgment

The research leading to these results has received funding by the Flagship Project RITMARE - The Italian Research for the Sea - coordinated by the Italian National Research Council and funded by the Italian Ministry of Education, University and Research within the National Research Program 2011-2013.

References

[1] L. Hernquist and N. Katz, "Treesph: A unification of sph with the hierarchical tree method," *Astrophysical Journal Supplement*, vol. 70, pp. 419–446, 1989.

[2] J. Bonet and M. Rodriguez-Paz, "Hamiltonian formulation of the variable-h sph equations," *J. Comp. Phys.*, vol. 209, pp. 541–558, 2005.

[3] R. Vacondio, B. Rogers, P. Stansby, P. Mignosa, and J. Feldman, "Variable resolution for sph: a dynamic particle coalescing and splitting scheme," *Computer Methods in Applied Mechanics and Engineering*, 2013.

[4] M. Lastiwka, N. Quinlan, and M. Basa, "Adaptive particle distribution for smoothed particle hydrodynamics," *International Journal for Numerical Methods in Fluids*, vol. 47, no. 10-11, pp. 1403–1409, 2005.

[5] J. Feldman and J. Bonet, "Dynamic refinement and boundary contact forces in SPH with applications in fluid flow problems," *International Journal for Numerical Methods in Engineering*, vol. 72, no. 3, pp. 295–324, 2007.

[6] G. Bulian, A. Souto-Iglesias, L. Delorme, and E. Botia-Vera, "SPH simulation of a tuned liquid damper with angular motion," *Journal of Hydraulic Research*, vol. 48, no. Extra Issue, pp. 28–39, 2010.

[7] S. Attaway, M. Heinstein, and J. Swegle, "Coupling of smooth particle hydrodynamics with the finite element method," *Nuclear Engineering and Design*, vol. 150, no. 2–3, pp. 199–205, 1994.

[8] C. Kassiotis, R. B.D., M. Ferrand, D. Violeau, S. B. K., and M. Benoit, "Strong coupling between 2d sph and 1d finite difference boussinesq solvers," in *6th ERCOFTAC SPHERIC workshop on SPH applications*, 2011.

[9] H. Takeda, S. M. Miyama, and M. Sekiya, "Numerical simulation of viscous flow by Smoothed Particle Hydrodynamics," *Progress of Theoretical Physics*, vol. 92, no. 5, pp. 939–960, 1994.

[10] E. M. Ryan, A. M. Tartakovsky, and C. Amon, "A novel method for modeling neumann and robin boundary conditions in smoothed particle hydrodynamics," *Computer Physics Communications*, vol. 181, no. 12, pp. 2008–2023, 2010.

[11] F. Macià, M. Antuono, L. M. González, and A. Colagrossi, "Theoretical analysis of the no-slip boundary condition enforcement in SPH methods," *Progress of Theoretical Physics*, vol. 125, no. 6, pp. 1091–1121, 2011. [Online]. Available: http://ptp.ipap.jp/link?PTP/125/1091/

[12] I. Federico, S. Marrone, A. Colagrossi, F. Aristodemo, and M. Antuono, "Simulating 2d open-channel flows through an sph model," *European Journal of Mechanics-B/Fluids*, vol. 34, pp. 35–46, 2012.

[13] S. Marrone, M. Antuono, A. Colagrossi, G. Colicchio, D. L. Touzé, and G. Graziani, "delta-sph model for simulating violent impact flows," *Computer Methods in Applied Mechanics and Engineering*, vol. 200, no. 13-16, pp. 1526 – 1542, 2011. [Online]. Available: http://www.sciencedirect.com/science/article/pii/S0045782510003725

[14] A. Colagrossi, B. Bouscasse, M. Antuono, and S. Marrone, "Particle packing algorithm for SPH schemes," *Computer Physics Communications*, vol. 183, no. 2, pp. 1641–1683, 2012.

[15] G. Dilts, "Moving-least-squares-particle hydrodynamics - i. consistency and stability," *International Journal for Numerical Methods in Engineering*, vol. 44, no. 8, pp. 1115–1155, 1999.

[16] B. Bouscasse, A. Colagrossi, S. Marrone, and M. Antuono, "Nonlinear water wave interaction with floating bodies in sph," *Accepted for publication, Journal of Fluids and Structures*, 2013.

[17] A. Colagrossi, A. Souto-Iglesias, M. Antuono, and S. Marrone, "Smoothed-particle-hydrodynamics modeling of dissipation mechanisms in gravity waves," *Phys. Rev. E*, vol. 87, p. 023302, Feb 2013. [Online]. Available: http://link.aps.org/doi/10.1103/PhysRevE.87.023302

[18] M. Antuono and A. Colagrossi, "The damping of viscous gravity waves," *Wave Motion*, no. 0, pp. –, 2012. [Online]. Available: http://www.sciencedirect.com/science/article/pii/S0165212512001060

[19] A. Di Mascio, R. Broglia, and R. Muscari, "On the application of the single-phase level set method to naval hydrodynamic flows," *Computers & fluids*, vol. 36, no. 5, pp. 868–886, 2007.

[20] R. Muscari, A. Di Mascio, and R. Verzicco, "Modelling of vortex dynamics in the wake of a marine propeller," *Computers & Fluids*, 2012.